Dynamical properties of a confined diatomic fluid undergoing zero mean oscillatory flow: Effect of molecular rotation

J. S. Hansen*
Centre for Molecular Simulation, Swinburne University of Technology, P.O. Box 218, Hawthorn, Victoria 3122, Australia

B. D. Todd†
Centre for Molecular Simulation, Swinburne University of Technology, P.O. Box 218, Hawthorn, Victoria 3122, Australia

Peter J. Daivis‡
Applied Physics, School of Applied Sciences, RMIT University, G.P.O. Box 2476V, Melbourne, Victoria 3001, Australia
(Received 6 September 2007; revised manuscript received 17 December 2007; published 19 June 2008)

In this paper we investigate the spatiotemporal dynamics of a diatomic fluid undergoing zero mean oscillatory flow in a slit pore. The study is based on nonequilibrium molecular dynamics simulations together with two limiting solutions to the Navier-Stokes equations which include the effect of molecular rotation. By examining the viscoelastic properties of the system we can estimate the extent of the Newtonian regime, and a direct comparison between the molecular dynamics data and the solutions to the Navier-Stokes equations is then possible. It is found that the agreement is excellent, and that the vortex viscosity can be estimated by fitting the data obtained in the molecular dynamics simulations to the solutions to the Navier-Stokes equations. The quantitative effect of the coupling between the linear momentum and the spin angular momentum on flow is also investigated. We find that the maximum flow can be reduced up to 3–4 % due to the coupling.

DOI: 10.1103/PhysRevE.77.066707 PACS number(s): 47.11.Mn, 47.10.ad, 05.20.Jj, 05.60.−k

I. INTRODUCTION

Classical fluid dynamics is concerned with the spatiotemporal dynamics of the fluid density, linear (or translational) momentum, and energy [1]. In this description these three quantities are coupled together via the balance equations, and by applying the phenomenological constitutive relations the corresponding Navier-Stokes formulation forms a closed set of equations [1,2], together with an equation of state [3]. The Navier-Stokes approach can be used to describe, for example, the air flow over an aircraft wing or an alkane fluid flowing in a microchannel. While such general theory is elegant, it excludes all microscopic dynamical features present in the system. Moreover, it ignores the coupling between the internal molecular degrees of freedom and the macroscopic quantities, e.g., the coupling between the molecular rotation and the fluid's translational momentum [4,5]. Only in very few situations can the coupling between the internal molecular degrees of freedom and the translational motion be safely ignored; however, this is not the situation in general. Nevertheless, it has become "the standard" to ignore this coupling and thereby also dismiss all the information about the microscopic degrees of freedom.

While this fact is well known, no one has, to our knowledge, performed any quantitative investigation estimating the error introduced when ignoring this coupling. Evans and Streett [6], Travis *et al.* [7,8], Delhommelle and Evans [9], and Radzyner and Rapaport [10] have studied rigid bonded diatomic molecular fluids undergoing a steady Poiseuille flow. For this problem it is possible to solve the extended Navier-Stokes equations, which include the coupling between the molecular rotation and the translational momentum [4]. These studies were all based on a comparison between nonequilibrium molecular dynamics (NEMD) simulations and the solution to the Navier-Stokes equations. It was shown that the extended Navier-Stokes theory qualitatively agreed with the NEMD results, except near the wall-fluid boundary, where large velocity slip, molecular alignment, and density variations are present. However, as we will discuss later, one cannot expect that the molecular rotation has a large (if any) effect on the translational momentum when the fluid flows in a steady manner. That is, the flow profile is neither qualitatively nor quantitatively different from that of the corresponding simple atomic fluid. This is not the case for unsteady flows, e.g., a zero mean oscillatory flow. Knowledge of the effect of the coupling may therefore be very relevant when manufacturing mixing devices and micropumping mechanisms [11,12].

The purpose of this paper is therefore threefold: (i) to solve the Navier-Stokes equations for a zero mean oscillatory flow including the coupling between the molecular rotation and the translational momentum, (ii) to perform NEMD simulations of a diatomic fluid undergoing such flow and validate the Navier-Stokes solution against simulation data, and (iii) to quantitatively analyze the effect of molecular rotation on the translational momentum. In order to accomplish this, the paper is organized as follows. In Sec. II we derive and present two limiting solutions to the Navier-Stokes equations. Section III briefly describes the details connected with the molecular dynamics simulations, and in Sec. IV we discuss the results and highlight the effect of the molecular rotation. Section V is devoted to conclusions.

*jhansen@ict.swin.edu.au
†btodd@swin.edu.au
‡peter.daivis@rmit.edu.au

II. LIMITING SOLUTIONS TO THE NAVIER-STOKES EQUATIONS

In the Appendix we derive the Navier-Stokes equations, which include the coupling between the streaming spin angular momentum **s** and the streaming velocity **u**. In the case of an incompressible fluid and in the absence of any applied external torque these are

$$\rho\frac{d\mathbf{u}}{dt} = \rho\mathbf{F}_e - \nabla p + (\eta_0 + \eta_r)\nabla^2\mathbf{u} + 2\eta_r(\nabla \times \mathbf{w}), \tag{1}$$

$$\rho\frac{d\mathbf{s}}{dt} = 2\eta_r(\nabla \times \mathbf{u} - 2\mathbf{w}) + (\zeta_v + \zeta/3 - \zeta_r)\nabla(\nabla \cdot \mathbf{w}) + (\zeta + \zeta_r)\nabla^2\mathbf{w}, \tag{2}$$

where ρ is the mass density, $\mathbf{F}_e$ is the external force per unit mass, $\mathbf{w}$ is the streaming angular velocity, η_0 and η_r are the shear and the vortex viscosities, and ζ, ζ_v, and ζ_r are the vortex spin viscosities. The streaming spin angular momentum is given by $\mathbf{s}=\Theta\cdot\mathbf{w}$, which for uniaxial molecules reduces to [7]

$$\mathbf{s} = \Theta\mathbf{w} \tag{3}$$

where Θ is the average of the trace of the inertia tensor $\mathbf{\Theta}$. Now, we let the fluid be confined between two planar walls and the direction of confinement be the y direction. We shall think of the x and z directions as being of infinite extent. A force $F_e(t)$ acts on the fluid in the x direction and, since the system is homogeneous in the x direction, the pressure gradient in this direction is zero. The force has a sufficiently low amplitude such that the streaming velocity is in the x direction only. In this case the Navier-Stokes equations reduce to

$$\frac{\partial u_x(y,t)}{\partial t} = F_e(t) + (\nu_0 + \nu_r)\frac{\partial^2 u_x(y,t)}{\partial y^2} + 2\nu_r\frac{\partial w_z(y,t)}{\partial y}, \tag{4}$$

$$\Theta\frac{\partial w_z(y,t)}{\partial t} = -2\nu_r\left(\frac{\partial u_x(y,t)}{\partial y} + 2w_z(y,t)\right) + (\xi + \xi_r)\frac{\partial^2 w_z(y,t)}{\partial y^2}, \tag{5}$$

where $u_x(y,t)$ is the streaming velocity in the x direction, $w_z(y,t)$ is the z component of the streaming angular velocity, ν_0 is the kinematic shear viscosity, ν_r is the kinematic vortex viscosity, and ξ and ξ_r are the kinematic vortex spin viscosities. Note, that due to the geometry and the low external force amplitude, $\nabla\cdot\mathbf{w}=0$.

Before we continue it would be of interest to estimate the contributions of the two terms on the right-hand side of Eq. (5). According to Evans and Streett [6] and Evans and Hanley [13], the vortex viscosity for liquid nitrogen is $\eta_r=4\times10^{-5}$ kg m^{-1} s^{-1} and the vortex spin viscosities are $\zeta=3\times10^{-24}$ kg m s^{-1} and $\zeta_r=2\times10^{-24}$ kg m s^{-1}. This indicates that the diffusion term in Eq. (5) can be ignored even for relatively large gradients in the streaming angular velocity:

$$\Theta\frac{\partial w_z(y,t)}{\partial t} \approx -2\nu_r\left(\frac{\partial u_x(y,t)}{\partial y} + 2w_z(y,t)\right). \tag{6}$$

For steady flows $\partial w_z(y)/\partial t=0$, which means that $2w_z(y)=-du(y)/dy$ or

$$\frac{dw_z(y)}{dy} = -\frac{1}{2}\frac{d^2u_x(y)}{dy^2}. \tag{7}$$

Substituting this relation into Eq. (4), we see that the two terms involving ν_r cancel, and we end up with the usual Navier-Stokes equation for a steady flow:

$$\frac{\partial^2 u_x(y,t)}{\partial y^2} = -\frac{F_e}{\nu_0}. \tag{8}$$

Thus, there is no effect of the molecular rotation on the streaming velocity.

We therefore wish to study an unsteady flow. We will here investigate the simple case where the external force field is a trigonometric function of time, $F_e(t)=F_0\cos(\omega t)$, where F_0 is the force amplitude and ω is the angular frequency of the force. The problem is simplified considerably by adopting complex notation, in which case

$$F_e(t) = \mathrm{Re}(F_0 e^{i\omega t}). \tag{9}$$

Since we are interested in the limiting behavior $t\to\infty$, i.e., where the transients have decayed and the oscillatory flow exhibits steady amplitude, both the streaming velocity and the streaming angular velocity are written as products of a spatial function and an oscillatory temporal factor with the same frequency as the external force field. In complex notation,

$$u_x(y,t) = \mathrm{Re}[U(y)e^{i\omega t}], \tag{10}$$

$$w_z(y,t) = \mathrm{Re}[W(y)e^{i\omega t}]. \tag{11}$$

Substituting Eqs. (10), (11), and (9) into Eqs. (4) and (5), we obtain

$$i\omega U(y) = F_0 + (\nu_0 + \nu_r)\frac{d^2U(y)}{dy^2} + 2\nu_r\frac{dW(y)}{dy}, \tag{12}$$

$$i\omega\Theta W(y) = -2\nu_r\left(\frac{dU(y)}{dy} + 2W(y)\right) + (\xi + \xi_r)\frac{d^2W(y)}{dy^2}. \tag{13}$$

It is possible to solve this inhomogeneous second-order differential equation system, but the solution is algebraically very involved and uninformative. We therefore turn to limiting solutions.

A. The limit $\xi+\xi_r\to0$

As just described above, it is a reasonable approximation to ignore the diffusion term in Eq. (5). This assumption can fail, especially near the wall-fluid boundary; nevertheless, it enables a very simple solution. Equation (13) yields

$$W(y) = -\frac{2\nu_r}{i\omega\Theta + 4\nu_r}\frac{dU(y)}{dy}. \tag{14}$$

Differentiating both sides and inserting the result into Eq. (12), one obtains an inhomogeneous second-order differential equation:

$$i\omega U(y) - \left(\nu_0 + \nu_r - \frac{4\nu_r^2}{i\omega\Theta + 4\nu_r}\right)\frac{d^2U(y)}{dy^2} = F_0. \tag{15}$$

Applying nonslip boundary conditions $[U(0)=U(2R)=0$, where R is half the channel width] and Eq. (10), the solution for the streaming velocity is

$$u_x(y,t) = \mathrm{Re}\left[\frac{F_0}{i\omega}\left(1 + \frac{e^{2\lambda' R} - 1}{\sinh(2\lambda' R)}\sinh(\lambda' y) - e^{\lambda' y}\right)e^{i\omega t}\right], \tag{16}$$

where

$$\lambda' = \left(\frac{\omega(4i\nu_r - \omega\Theta)}{i\omega\Theta(\nu_0 + \nu_r) + 4\nu_r\nu_0}\right)^{1/2}. \tag{17}$$

The streaming angular velocity is given from Eq. (14):

$$w_z(y,t) = \mathrm{Re}\left[-\frac{2\nu_r\lambda' F_0}{\omega^2\Theta + 4\nu_r i\omega} \times\left(\frac{e^{2\lambda' r} - 1}{\sinh(2\lambda' r)}\cosh(\lambda' y) - e^{\lambda y}\right)e^{i\omega t}\right]. \tag{18}$$

B. The limit $\omega \to 0$

For sufficiently small channel width and small external force frequency, i.e., essentially a Poiseuille flow with a quadratic velocity profile, the differential equation system given by Eqs. (12) and (13) can be solved analytically by applying nonslip boundary conditions. In this situation the streaming angular velocity is given by the functional form [4]

$$W(y) = \frac{u_c}{R}\left(\frac{y}{R} - 1 - \frac{\sinh[K(y-R)]}{\sinh(KR)}\right), \tag{19}$$

where K has units of inverse length and u_c of length per unit time, i.e., velocity. Both K and u_c are function (or model) parameters that must be fitted from data obtained by NEMD simulations, for example. If we inspect Eq. (19), we see that $W(y)$ consists of a linear part and a hyperbolic part. For large values of K, i.e., $K \gg 1$, the hyperbolic term is significant only near the wall-fluid boundary, where it forces the angular velocity to zero in accordance with the boundary conditions. The angular velocity in the interior of the channel will then be given as a linear function of y with slope u_c/R^2, which in turn means that u_c depends on the ratio between the external force and the viscosity, i.e., $u_c \propto F_e/\nu_0$, in agreement with the case of a steady Poiseuille flow. For $K < 1$ the hyperbolic term will dominate the behavior of $W(y)$ for all y. Thus, K is a constant that describes how the effect from the wall on the angular velocity extends into the channel. This means that small values of K indicate large wall penetration depth and large values of K indicate small penetration. See also Ref. [8] for a discussion of steady flows.

As stated above, the functional form is based on the assumption that the streaming velocity is quadratic with respect to the spatial coordinate. This assumption means that the viscous force is dominating, which can be quantified via the Stokes parameter, which is often used to characterize oscillatory flows [14]. We will here define it as $\Lambda = \sqrt{\omega/2(\nu_0+\nu_r)}R$. Thus, for sufficiently small Stokes parameter, Eq. (19) is valid. In the simulations R never approaches zero, so we will therefore simply let $\omega \to 0$ when we study the fluid for small Stokes parameter. In the case where the inertia forces dominate (large Stokes parameter), the velocity profiles will exhibit spatial oscillations, and in the limit of a purely inviscid fluid flow ($\Lambda \to \infty$) the velocity profile will be flat and vary only with respect to time.

Now, adopting the limiting solution to the streaming angular velocity, we substitute Eq. (19) into Eq. (12) and obtain a simple inhomogeneous second-order differential equation,

$$i\omega U(y) - (\nu_0 + \nu_r)\frac{d^2U(y)}{dy^2} = F_0 + \frac{2\nu_r u_c}{R^2}\left(1 - \frac{KR\cosh[K(y-R)]}{\sinh(KR)}\right), \tag{20}$$

which we will assume satisfies nonslip boundary conditions. The solution to this problem is given by

$$U(y) = A\left(1 - e^{\lambda y} + \frac{e^{2\lambda R} - 1}{\sinh(2\lambda R)}\sinh(\lambda y)\right) + B\cosh(KR)\left(e^{\lambda y} - \frac{e^{2\lambda} - 1}{\sinh(2\lambda R)}\sinh(\lambda y)\right) - B\cosh[K(y-R)], \tag{21}$$

where

$$\lambda = \left(\frac{i\omega}{\nu_0 + \nu_r}\right)^{1/2}, \tag{22}$$

$$A = \frac{F_0 R^2 + 2\nu_r u_c}{i\omega R^2}, \tag{23}$$

$$B = \frac{2\nu_r u_c K}{R[(\nu_0 + \nu_r)K^2 - i\omega]\sinh(KR)}. \tag{24}$$

The solution for the streaming velocity in the limits $\Lambda \to 0$ and $t \to \infty$ is then given by

$$u_x(y,t) = \mathrm{Re}\left[A\left(1 - e^{\lambda y} + \frac{e^{2\lambda R} - 1}{\sinh(2\lambda R)}\sinh(\lambda y)\right)e^{i\omega t} + B\cosh(KR)\left(e^{\lambda y} - \frac{e^{2\lambda} - 1}{\sinh(2\lambda R)}\sinh(\lambda y)\right)e^{i\omega t} - B\cosh[K(y-R)]ei\omega t\right]. \tag{25}$$

It is important to observe that $A = F_0/i\omega$ for $\nu_r = 0$ and $\lim_{\nu_r \to 0} B = 0$. In this situation Eq. (25) reduces to the solu-

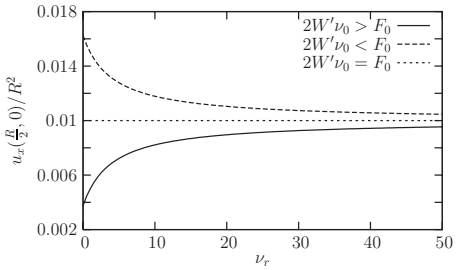

FIG. 1. Streaming velocity in the center of the channel as a function of the kinematic vortex viscosity for different values of F_0: $F_0=2W'\nu_0+0.05$ (broken line), $2W'\nu_0-0.05$ (full line), and $2W'\nu_0$ (dotted line); $W'=0.01$ and $\nu_0=4.0$.

tion of an atomic fluid with no molecular spin; see, for example, Engelund [14,15]. Also note that λ is related to the Stokes parameter by $\lambda=\sqrt{2i}\Lambda/R$. The spatiotemporal dynamics of the streaming angular velocity is given directly by Eqs. (11) and (19):

$$w_z(y,t)=\mathrm{Re}\left[\frac{u_c}{R}\left(\frac{y}{R}-1-\frac{\sinh[K(y-R)]}{\sinh(KR)}\right)e^{i\omega t}\right]. \quad (26)$$

We have compared Eqs. (25) and (16) with the numerical solution of the Navier-Stokes equations (4) and (5), using an Euler finite-difference method. This shows very good agreement over a range of reasonable parameter values where $\nu_r \ll \nu_0$, a relation which is expected from the literature [6,16].

C. A few additional remarks

It is instructive to see the effect of the molecular spin on the streaming velocity. This can be achieved by a particularly simple example. For very large values of K (i.e., small wall effects), $B\approx 0$, leaving only the first term on the right-hand side in Eq. (25) relevant. This approximation effectively means that the streaming angular velocity is a linear function of y: $w_z(y,t)=W'(y-R)\cos(\omega t)$, where $W'=u_c/R^2$ is the slope of the angular velocity with respect to y. In nanofluidic systems the viscous forces will typically dominate, which means that the Stokes parameter is relatively small. This justifies a Taylor expansion of the exponential and hyperbolic functions to second order in λ. Inserting these expansions into the first term in Eq. (25) we obtain

$$u_x(y,t)=\frac{F_0+2\nu_r W'}{2(\nu_0+\nu_r)}y(2R-y)\cos(\omega t). \quad (27)$$

A similar approximation can also be found expanding Eq. (16). It can now be seen that, for low Stokes parameter and for large values of K, the streaming velocity is characterized by a quadratic spatial variation which corresponds to a temporally oscillating Poiseuille flow. More importantly, from this solution we can identify three different scenarios: At any point y, the amplitude of the streaming velocity increases with respect to ν_r if $2W'\nu_0>F_0$, decreases if $2W'\nu_0<F_0$, and is constant if $2W'\nu_0=F_0$. This is illustrated in Fig. 1, where the streaming velocity in the middle of the channel is plotted as a function of the vortex viscosity for the three different scenarios. This can also be understood from Eq. (4), where the vortex viscosity enters in the diffusion term, which will contribute to a decrease in the streaming velocity, and in the coupling term, which contributes to an increase in the streaming velocity. It is then the difference between F_0 and $2W'\nu_0$ that determines the effects of ν_r. From Fig. 1 another important point is observed: The streaming velocity amplitude is highly dependent on ν_r for low values of ν_r; however, for high values the streaming velocity converges slowly toward $W'R^2$.

III. MOLECULAR DYNAMICS SIMULATIONS

The method for simulating an external force acting on a confined fluid via NEMD is well developed by now (see Refs. [17–19]), and we will here only briefly summarize the computational methodology. The system is composed of a fluid confined between two walls such that the direction of confinement is the y direction. The wall atoms are initially arranged on hexagonal packed planes, where the distance between the planes is 0.8σ, σ being a measure of length and around one atomic diameter, i.e., 3–4 Å. The wall atoms are kept around their initial (or equilibrium) positions via a restoring spring force $\mathbf{F}(\mathbf{r}_i(t))=-k[\mathbf{r}_{\mathrm{eq}}-\mathbf{r}_i(t)]$. $k=100$ is the spring constant, $\mathbf{r}_i(t)$ is the position of atom i, and $\mathbf{r}_{\mathrm{eq}}$ is the equilibrium position. Any physical quantity is expressed in appropriate units of energy ϵ, mass m, and length σ, traditionally used in molecular dynamics simulations; see, for example, Ref. [20]. We shall omit writing these units explicitly throughout the paper and simply set $\epsilon=m=\sigma=1$. In order to decrease the computational effort, we apply periodic boundary conditions in all directions, such that a single wall will act as a first and second wall [17,19]. The wall is made up of three hexagonal layers in the y direction and has number density $\rho_w=0.868$. The molecules are composed of $N_b=2$ united atom units (UAU) or atoms. We shall here use the term "atom" for both of these units. In the simulations the overall atom number density is $\rho=0.73$ giving a molecular density of $\rho_m=0.365$. All atoms (including wall atoms) interact via the Weeks-Chandler-Andersen (WCA) pair potential [21]

$$U^{\mathrm{WCA}}(r_{ij})=\begin{cases}4(r_{ij}^{-12}-r_{ij}^{-6})+1 & \text{if } r_{ij}\le 2^{1/6},\\ 0 & \text{otherwise,}\end{cases} \quad (28)$$

where r_{ij} is the distance between the two atoms. The atoms comprising the diatomic molecules are connected via the finitely extensible nonlinear elastic (FENE) potential [22]

$$U^{\mathrm{FENE}}(r_{ij})=-\frac{1}{2}k_0R_0^2\ln[1-(r_{ij}/R_0)^2], \quad r_{ij}\le R_0. \quad (29)$$

$k_0=30$ is a spring constant and $R_0=1.5$ is the maximum bond length. The choice of these values is based on previous work [18]. The fluid atoms are subjected to a temporally oscillatory external force field in the x direction, $\mathbf{F}_e(t)=(F_0\cos(\omega t),0,0)$, where $\omega=2\pi/50$ or $2\pi/200$. The wall atoms are coupled to a Nosé-Hoover thermostat [23,24] such that the heat generated in the fluid due to the viscous flow is conducted away from the system at the wall-fluid boundary. Since the external force amplitude is relatively small, the

heat conduction at the wall ensures that the fluid temperature is constant in time and space and equal to that of the wall, which is $T=1.0$. In principle, very small spatiotemporal variations will be present; however, these are so small that they will not affect the transport properties of the fluid. The numbers of particles are 1800–4200 depending on the channel width. The equations of motion for the atoms are integrated forward in time by the leapfrog integration scheme [20] using a time step of 0.0025. The system is run for 2×10^5 time steps before sampling. After this initial period the average momentum exhibits stable amplitude oscillations.

All the physical quantities are measured as spatiotemporal averages in bins with volume $V_{\text{bin}}=L_x\Delta yL_z$, where L_x and L_z are the lengths of the simulation box in the x and z directions and $\Delta y=0.1$ is the bin width in the y direction. In order to increase the signal to noise ratio to a satisfactory level, we divide the external force field period into eight equally long time intervals, e.g., if the period is 50, $t_{n+1}-t_n=\Delta t=50/8$, where $n=1,\ldots,8$. If we assume that Δy is sufficiently small we can formally write the average of a physical quantity x in bin j in the time interval $t_n\leq t\leq t_{n+1}$ as

$$\bar{x}_j=\frac{1}{\Delta t}\int_{t_n}^{t_{n+1}}\left(\sum_{i=1}^{N}x_i\int_{y_n}^{y_{n+1}}\delta(y_i(t)-y_j)dy\right)dt$$
$$=\frac{1}{\Delta t}\int_{t_n}^{t_{n+1}}x_j(t)dt, \tag{30}$$

where x_i is the corresponding molecular quantity of molecule i, y_j is the bin midpoint, and $y_i(t)$ is the center of mass and $y_{n+1}-y_n=\Delta y$. $x_j(t)$ is then the value in bin j. In practice, we obtain $\bar{x}_j$ using sample averages reducing this to a simple (spatiotemporal) two-dimensional histogram method.

IV. RESULTS AND DISCUSSION

A. Viscoelastic properties

Before we present the results from the NEMD simulations and compare the data with the Navier-Stokes solutions, we must (i) make sure that we are in the Newtonian regime where the viscosities are independent of the frequency and amplitude of the external force, (ii) make sure that the frequency is sufficiently low such that any relaxation phenomena can be safely ignored, and (iii) obtain independent values for the transport coefficients such that these can be used in the analysis as well as be compared with the results from the NEMD simulations. The zero-frequency zero-wave-vector kinematic viscosities entering the Navier-Stokes equations can be estimated via a separate equilibrium molecular dynamics (EMD) simulation using the Green-Kubo integral of the autocorrelation functions of the relevant parts of the pressure tensor [25]. The pressure tensor itself can be expressed in the molecular or in the atomic formalism, and it has been shown by several authors that the integrals of the autocorrelation functions of the pressure tensors converge to the same value for sufficiently long times [26,27]. This is despite the fact that the correlation functions themselves are different. The molecular approach is often advantageous since the autocorrelation function is smooth and faster decaying because it does not explicitly include the effects of high-frequency bond stretching, bond bending, etc. [28]. Furthermore, the rotational viscosity is calculated using the antisymmetric part of the molecular pressure tensor [6], and we therefore apply this formalism when evaluating the zero-frequency zero-wave-vector viscosities. The molecular pressure tensor is microscopically given as [26]

$$\mathbf{P}(t)=\frac{1}{V}\sum_i\left(\frac{\mathbf{p}_i(t)\mathbf{p}_i(t)}{M_i}+\sum_{j>i}\mathbf{r}_{ij}(t)\mathbf{F}_{ij}(t)\right), \tag{31}$$

where V is the volume, $\mathbf{p}_i(t)$ is the momentum of the center of mass of molecule i, M_i is the total mass of the molecule, $\mathbf{r}_{ij}(t)=\min(\mathbf{r}_i-\mathbf{r}_j)$ is the minimum periodic image vector distance between the center of mass of molecules i and j, and $\mathbf{F}_{ij}(t)$ is the total force on molecule i due to all molecules j. This force is

$$\mathbf{F}_{ij}(t)=\sum_{\alpha\in i}\sum_{\beta\in j}\mathbf{F}_{i\alpha j\beta}(t), \tag{32}$$

where $\mathbf{F}_{i\alpha j\beta}(t)$ is the force acting between atom α in molecule i and atom β in molecule j. The kinematic shear viscosity is then given directly by the equilibrium Green-Kubo integral [6,29]:

$$\nu_0=\frac{V}{10k_BT\rho}\int_0^\infty\left\langle\overset{os}{\mathbf{P}}(0):\overset{os}{\mathbf{P}}(t)\right\rangle dt, \tag{33}$$

where $\overset{os}{\mathbf{P}}(t)=\frac{1}{2}[\mathbf{P}(t)+\mathbf{P}^T(t)]-\frac{1}{3}\text{tr}[\mathbf{P}(t)]\mathbf{1}$ is the traceless symmetric part of the pressure tensor, V is the simulation volume, and k_B is the Boltzmann constant.

Since the spin angular momentum is a nonconserved quantity the vortex viscosity cannot be evaluated by a simple Green-Kubo relation, but can be found by solving the generalized Langevin equation [13]. From this the Laplace transform of the vortex viscosity is given by [13]

$$\tilde{\eta}_r(s)=\frac{\tilde{c}(s)}{1-\frac{4}{\rho\Theta}\frac{\tilde{c}(s)}{s}}. \tag{34}$$

$\tilde{c}(s)$ is the Laplace transform of the antisymmetric stress autocorrelation function:

$$\tilde{c}(s)=\frac{V}{3k_BT}\int_0^\infty\left\langle\overset{d}{\mathbf{P}}(0)\cdot\overset{d}{\mathbf{P}}(t)\right\rangle e^{-st}dt. \tag{35}$$

where $\overset{d}{\mathbf{P}}$ is the vector dual of the antisymmetric part of the pressure tensor (see the Appendix). As pointed out by Evans and Hanley [13], using molecular dynamics data and Eq. (35) directly together with the relation in Eq. (34) will lead to large numerical uncertainties for $s\to0$. To avoid this, the authors assumed the functional form

$$\tilde{\eta}_r(s)=\frac{\tilde{\eta}_r(0)}{1+s\tau}, \tag{36}$$

where τ is the relaxation time. Substituting this into Eq. (34) and rearranging yields

$$\tilde{c}(s) = \frac{\tilde{\eta}_r(0)s}{s + s^2\tau + \frac{4}{\rho\Theta}\tilde{\eta}_r(0)}. \quad (37)$$

One can then fit the EMD data of $\tilde{c}(s)$ to Eq. (37) using τ and $\tilde{\eta}_r(0)$ as fitting parameters.

The Navier-Stokes equations are based on the assumption that the system is in the Newtonian regime, where the shear viscosity is independent of the external force frequency. While the molecular and the atomic formalisms of the pressure tensor discussed above yield the same shear viscosities as $t \to \infty$, the two approaches differ greatly for small and intermediate times. We therefore turn to the atomic formalism when investigating the complex frequency-dependent shear viscosity, which is defined as [25]

$$\eta^*(\omega) = \eta'(\omega) + i\eta''(\omega) = \frac{V}{k_B T}\int_0^\infty \langle P_{xy}(0)P_{xy}(t)\rangle e^{-i\omega t}dt, \quad (38)$$

where $P_{xy}(t)$ is the xy atomic pressure tensor element and $\eta'(\omega)$ and $\eta''(\omega)$ are the real and imaginary parts of the viscosity, respectively. For the molecular fluid studied here P_{xy} is given by [26,30]

$$P_{xy} = \frac{1}{V}\sum_{i,\alpha}\left(\frac{p_{x,i\alpha}p_{y,i\alpha}}{m_{i\alpha}} + \frac{1}{2}\sum_{\substack{j,\beta \\ i\alpha \neq j\beta}} r_{x,i\alpha j\beta}F^{\mathrm{WCA}}_{y,i\alpha j\beta} + \frac{1}{2}\sum_{\substack{\beta \in i \\ \beta \neq \alpha}} r_{x,i\alpha i\beta}F^{\mathrm{FENE}}_{y,i\alpha i\beta}\right), \quad (39)$$

where $p_{x,i\alpha}(t)$ and $p_{y,i\alpha}(t)$ are the momenta in the x and y directions of the atom α in molecule i. $r_{x,i\alpha j\beta}$ is the minimum periodic distance in the x direction between atom α in molecule i and atom β in j.

For $T=1.0$, $\rho=0.73$, the kinematic viscosities are evaluated as $\nu_0 = 1.94 \pm 0.05$ and $\nu_r = 0.26 \pm 0.02$. The errors are based on one-half the maximum difference of five results. The low vortex viscosity is in agreement with earlier findings [13,16] and indicates that the molecular spin has only a small effect on the streaming velocity. As mentioned in Sec. II, the Navier-Stokes equations given in Eqs. (4) and (5) provide a complete description only if the chemical bond is rigid (and if we are in the Newtonian regime). Here we model flexible bonded molecules, and the stretching potential will affect the pressure tensor. However, we have found that the resulting vortex viscosity depends only slightly on this as long as the spring constant is sufficiently large.

To follow the notation often used in rheology, we plot the logarithm to the base 10 of the loss modulus $G''(\omega) = \omega\eta'(\omega)$ rather than the real part of the complex viscosity itself (Fig. 2). In the Newtonian regime $\log_{10}[G''(\omega)]$ should be a linear function of $\log_{10}(\omega)$ with a slope of 1. This is depicted in Fig. 2 as the broken line. We estimate that the frequency-independent Newtonian regime is when $\omega < 0.3$. Matin *et al.* [31] have investigated the strain rate dependence of the shear viscosity in a rigid bonded diatomic WCA fluid.

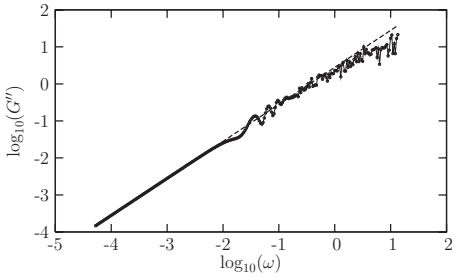

FIG. 2. Logarithm of the loss modulus $G''(\omega)$ versus the logarithm of the frequency ω. The broken line represents the Newtonian behavior.

They showed that for a system with molecular density of 0.42 and temperature of 1.0 shear thinning takes place for $\dot{\gamma} > 0.2$. We can calculate the strain rate in our simulations by numerical differentiation of the streaming velocity profiles, which will be presented later. From this, we observe that the strain rate in the interior of the channel is $\dot{\gamma} < 0.11$. Hence, the system is in the Newtonian regime.

Finally, we evaluate the relaxation time given by $\tau = \Psi_{1,0}/2\eta_0$, where $\Psi_{1,0}$ is the first normal stress coefficient in the limit of zero strain rate and is given via the relaxation modulus $G(t)$ [32]:

$$\Psi_{1,0} = 2\int_0^\infty tG(t)dt = \frac{2V}{10k_BT}\int_0^\infty t\left\langle \overset{os}{\mathbf{P}}(0):\overset{os}{\mathbf{P}}(t)\right\rangle dt. \quad (40)$$

This yields a relaxation time of around 0.07 ± 0.06. It is interesting to note that the relaxation time obtained using the fit in Eq. (37) is around 0.04. The system relaxation time is thus sufficiently low compared with the external force period that memory effects can be safely disregarded.

B. Dynamical properties

In Fig. 3 we plot the molecular number density ρ_m, multiplied by the number of atoms per molecule $N_b=2$. The density is defined for bin j as $\rho_{m,j}(t) = 1/M_i\Sigma_{i\in j}M_i$, where i runs over all molecules with center of mass located in the volume associated with bin j at time t. It is observed that, for the external force and frequencies examined here, the density profiles exhibit the same qualitative and quantitative behavior as the corresponding Poiseuille flow [18].

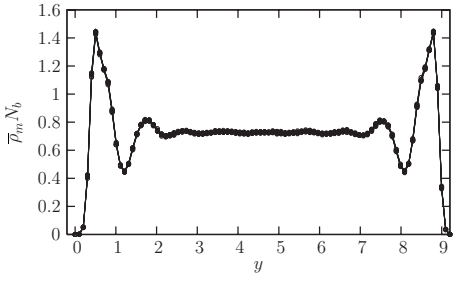

FIG. 3. Molecular density profiles $\bar{\rho}_m$ multiplied by $N_b=2$. $\omega = 2\pi/50$ and $F_0=0.1$. All eight profiles are shown and the data points are connected with lines as a guide to the eye.

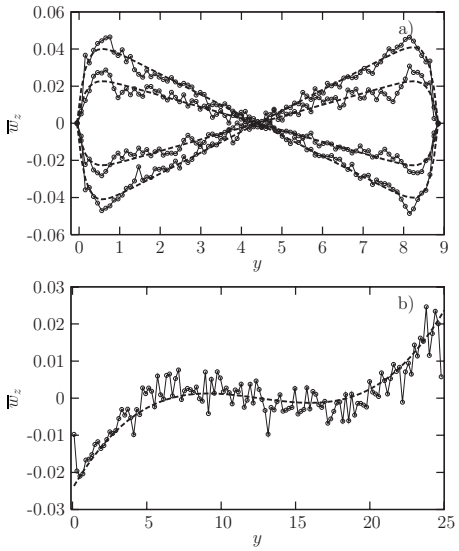

FIG. 4. (a) Streaming angular velocity profiles for four different time intervals where $\omega=2\pi/50$ and $\Lambda\approx0.75$ (circles with connecting lines). Punctured lines represent the fits to the time average of Eq. (26) where u_c and K are used as fitting parameters. (b) Angular streaming velocity profile for $\omega=2\pi/50$ and $\Lambda\approx2.28$ (circles with connecting lines). The broken line is the time average of the solution given in Eq. (18) where $\Theta=1.21$, $\nu_0=1.94$, and $\nu_r=0.25$. Only one profile is included for clarity.

The total molecular spin angular momentum per unit mass in bin j is given by [8]

$$\mathbf{s}_j(t)=\mathbf{\Theta}_j(t)\cdot\mathbf{w}_j(t), \tag{41}$$

where $\mathbf{\Theta}_j(t)$ is the total moment of inertia tensor per unit mass evaluated with respect to the center of mass. In the molecular dynamics simulations the molecular spin angular momentum and the moment of inertia are

$$\mathbf{s}_j(t)=\sum_{\substack{i,\alpha\\ i\in j}}\mathbf{r}_{i\alpha}(t)\times\mathbf{p}_{i\alpha}(t), \tag{42}$$

$$\mathbf{\Theta}_j(t)=\sum_{\substack{i,\alpha\\ i\in j}}\frac{m_{i\alpha}}{M_i}\{[\mathbf{r}_{i\alpha}(t)^2]\mathbf{1}-\mathbf{r}_{i\alpha}(t)\mathbf{r}_{i\alpha}(t)\}. \tag{43}$$

$\mathbf{r}_{i\alpha}(t)$ is the distance from the center of mass of atom α in molecule i, $\mathbf{p}_{i\alpha}(t)$ is the momentum, and $m_{i\alpha}$ is the mass of the atom. The angular streaming velocity is obtained from Eq. (41), noting that only the z vector component is nonzero. The results can be compared with the solutions to the Navier-Stokes equations, that is, from Eq. (30):

$$\bar{w}_z=\frac{1}{\Delta t}\int_{t_n}^{t_{n+1}}w_z(y,t)dt, \tag{44}$$

where $w_z(y,t)$ is given in either Eq. (26) or (18). In Fig. 4(a) we have plotted $\bar{w}_z$ obtained from the molecular dynamics simulations for four different time intervals where the angular frequency of the driving force is $2\pi/50$ and where the Stokes parameter is around 0.75. The value of the Stokes parameter is based on the viscosities found in Sec. IV A. From this we have compared the results with the best fit to the time average of Eq. (26). The parameters u_c and K are used as fitting parameters, and t is set such that Eq. (44) is in phase with the molecular dynamics results. The agreement is excellent except for points around $\sigma/2$ away from the wall. The reason for this is likely linked to the large density variation in this region (see Fig. 3). The best fit predicts values $u_c=0.3$ and $K=9$. It should also be noted that away from the wall $w_z\approx\frac{1}{2}\partial\bar{u}_x/\partial y$, which means that in the interior of the channel the effect from the wall on the molecular rotation vanishes. This is also indicated by the relatively large value of K. Figure 4(b) shows a streaming angular velocity profile for $\omega=2\pi/50$ and $\Lambda\approx2.28$ which is obtained by increasing the channel width but keeping the strain rate sufficiently low such that the system is in the Newtonian regime. This is achieved by setting $F_0=0.0425$. For this relatively large value of the Stokes parameter we cannot expect Eq. (26) to be valid, and the broken line represents the time average of Eq. (18) using ν_r as a fitting parameter. The parameter value for $\Theta=1.21$ is calculated directly in the NEMD simulations and $\nu_0=1.94$ which was found in the EMD simulations. This fit predicts $\nu_r=0.25$, in excellent agreement with the value of 0.26 ± 0.02 found previously from the equilibrium simulation.

It is here important to appreciate that this is information about the fluid that is traditionally excluded. For small values of the Stokes parameter, i.e., where the viscous forces are dominating, the molecular rotation is linear with respect to y. For large Stokes parameter, on the other hand, we observe a large variation in the molecular rotation as we move from the wall-fluid boundary into the interior of the channel; however, in the interior region the molecular rotation varies only slightly.

The molecular streaming velocity in bin j at time t is defined via $\mathbf{u}_j(t)=\Sigma_{i\in j}M_i\mathbf{v}_i(t)/\Sigma_{i\in j}M_i$, where $\mathbf{v}_i(t)$ is the center of mass velocity of molecule i with center of mass in bin j (see also [18]). In Fig. 5 we have plotted streaming velocity data for two different situations: Figs. 5(a) and 5(b) are for $\omega=2\pi/200$, giving $\Lambda\approx0.37$, and Figs. 5(c) and 5(d) are for $\omega=2\pi/50$ and $\Lambda\approx2.28$. In Figs. 5(a) and 5(b) the full lines represent the time average of the solution to the Navier-Stokes equation for low Stokes parameter, Eq. (25). In Figs. 5(c) and 5(d) the full lines are fits to Eq. (16). The parameter values used are found from the EMD simulations presented earlier. For Figs. 5(a) and 5(b) u_c and K were fitted in Fig. 4(a). The profiles allow slip boundary conditions, which we introduce in an *ad hoc* fashion:

$$\bar{u}_x=\frac{1}{\Delta t}\int_{t_n}^{t_{n+1}}[u_x(y,t)+u_0]dt, \tag{45}$$

where u_0 is the streaming velocity at the wall-fluid boundary. The molecular dynamics data and the solution to the Navier-Stokes equations show a very good agreement. It is important to stress that according to the discussion in Sec. IV A both systems are in the Newtonian regime. Another important point is that the limiting solution given in Eq. (16) also

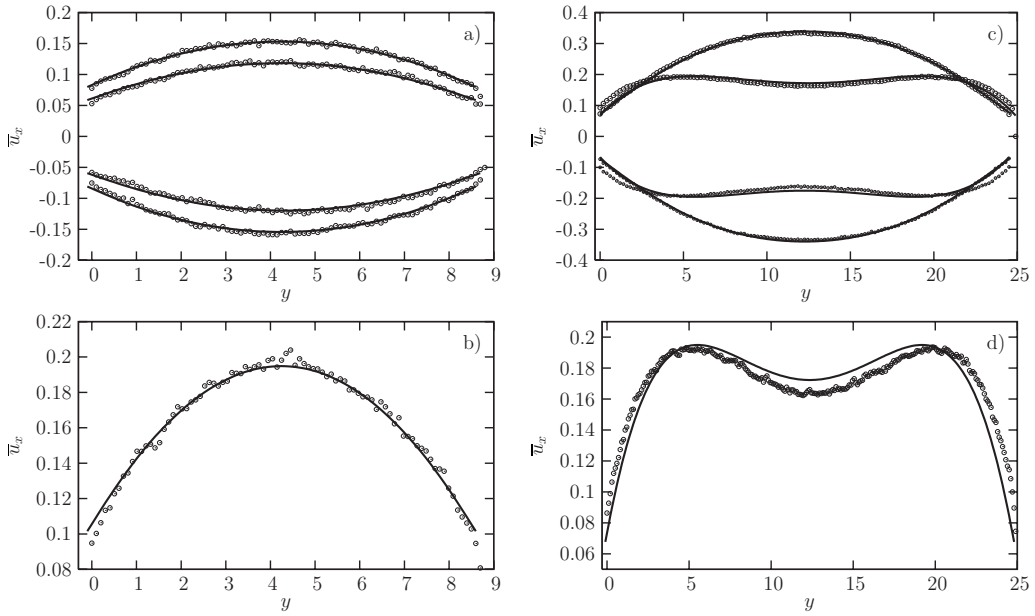

FIG. 5. (a) Streaming velocity profiles for four different time intervals (circles) where $\omega=2\pi/200$ and $\Lambda\approx0.37$. $F_e=0.02$. Full lines represent the time-averaged solution to the Navier-Stokes equation (25). The slip velocity u_0 is found to be 0.080, 0.058, −0.059, and −0.081. (b) Same as (a) but for a single time interval. $u_0=0.102$. (c) Streaming velocity profiles for four different time intervals (circles) where $\omega=2\pi/50$ and $\Lambda\approx2.28$. $F_e=0.0425$. Full lines are the time average of Eq. (16) using $\Theta=1.21$. The slip velocity u_0 is found to be 0.076, 0.071, −0.073, −0.075. (d) Same as for (c) but for a single time interval. $u_0=0.076$.

predicts satisfactory profiles for low values of Λ, indicating small wall effects.

We can now make a quantitative analysis of the effect of the coupling between the molecular rotation and the streaming velocity. To do so we define the maximum flow through the channel during the external force period as

$$Q_{\nu_r}^{\max}=\sup_{t\in[0;2\pi/\omega]}\int_0^{L_y}u_x(y,t)dy, \tag{46}$$

where $u_x(y,t)$ is given by either Eq. (16) or Eq. (25). Note that we underline the dependency of the vortex viscosity as a subscript. As we have shown earlier, it is not expected that the streaming velocity is much affected by the molecular rotation in the limit $\Lambda\to0$ and we shall therefore discuss only the case for $\xi+\xi_r\to0$, i.e., for Eq. (16). In Fig. 6 we have plotted $1-Q_{\nu_r}^{\max}/Q_{\nu_r=0}^{\max}$ as a function of ν_r/ν_0 for three

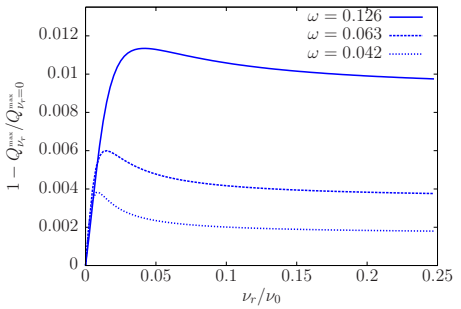

FIG. 6. (Color online) Effect of molecular rotation on the maximum fluid flow as a function of the ratio between the rotational and shear viscosities and the frequency. The curves are based on Eq. (16) using parameter values $\nu_0=1.94$, $F_e=0.1$, $R=6$, and $\Theta=1.21$.

different frequencies. First, we observe that the maximum flow in the channel decreases (the curves in Fig. 6 increase) as a function of ν_r/ν_0, that is, the coupling between the rotational and the translational motions will lead to a decrease in the maximum flow. This effect has a maximum, and it then slowly converges toward a plateau. This means that even for a fluid with a large vortex viscosity the effect will be rather limited, depending on the frequency. Second, and as expected, the molecular rotation seems to have an important effect on the flow for sufficiently large frequencies: the maximum flow may be reduced by more than 1% for $\omega=0.126$. For $\omega=2\pi$ (not shown in Fig. 6), the maximum flow is reduced by more than 3.5% if the frequency dependency of the transport coefficients is ignored.

V. CONCLUSION

In this paper we have investigated the fluid dynamics of a diatomic fluid undergoing zero mean oscillatory flow. Two limiting solutions to the Navier-Stokes equations that included the coupling between the spin angular and the translational momenta were presented. We showed that, for sufficiently low velocity slip at the wall-fluid boundary, the solutions for the streaming velocity could be augmented with a simple *ad hoc* slip and agreed very well with the molecular dynamics data. In addition to the obvious fact that this then allows us to extract additional information about the molecular rotation, it also enables us to study the coupling between the molecular rotation and streaming velocity. We showed that ignoring this coupling will lead to an error in the maximum flow of about 1% in the Newtonian regime, but can be much larger, more than 3.5%, for sufficiently high values of

ν_r if the frequency dependence of the viscosities can be ignored. It should be mentioned that there are many other ways of measuring the coupling effect. For example, the average flow over one-half the oscillation period will not be affected by more than a few tenths of a percent, whereas the maximum difference in the flow profile may be very large (more than 10%).

This work has been limited to the study of essentially rigid bonded diatomic molecules. The dynamical properties of more complex fluids could also be undertaken, e.g., fluids composed of *n*-alkanes, branched polymers, etc. In this case, however, one has to take care when constructing the Navier-Stokes equations, since the molecular details may have important effects on the fluid dynamics. For such complex fluids the spatiotemporal structural behavior also becomes interesting and phenomena such as molecular deformation and alignment could be studied.

ACKNOWLEDGMENT

The authors thank the Australian Research Council for supporting this work as part of a Discovery Grant (No. DP 0663759).

APPENDIX: DERIVATION OF THE NAVIER-STOKES EQUATION

In the case of zero temperature gradient, the relevant balance equations describing the mass density and the linear and angular momentum changes are (in nonconservation form) [6]

$$\frac{d\rho}{dt} = -\rho(\nabla \cdot \mathbf{u}), \tag{A1}$$

$$\rho\frac{d\mathbf{u}}{dt} = \rho\mathbf{F}_e - \nabla \cdot \mathbf{P}, \tag{A2}$$

$$\rho\frac{d\mathbf{s}}{dt} = \rho\boldsymbol{\Gamma}_e - \nabla \cdot \mathbf{Q} - 2\overset{d}{\mathbf{P}}. \tag{A3}$$

Here ρ is the mass density, $\mathbf{u}$ is the streaming velocity, $\mathbf{F}_e$ is the external force per unit mass, $\mathbf{P}$ is the pressure tensor, $\mathbf{s}$ is the spin angular momentum, $\boldsymbol{\Gamma}_e$ is the applied external torque per unit mass, and $\mathbf{Q}$ is the couple tensor. $\overset{d}{\mathbf{P}}$, which is the axial (or pseudo) vector dual of the antisymmetric part of the pressure tensor $\overset{a}{\mathbf{P}}$, can be written as

$$\overset{d}{\mathbf{P}} = \frac{1}{2}\boldsymbol{\epsilon} : \mathbf{P}^T = \left(\overset{a}{P}_{yz}, \overset{a}{P}_{zx}, \overset{a}{P}_{xy}\right), \tag{A4}$$

where $\boldsymbol{\epsilon}$ is the third-order Levi-Cività tensor, and $\overset{a}{P}_{\alpha\beta}$, where $\alpha, \beta \in x, y, z$, is the $\alpha\beta$ element of $\overset{a}{\mathbf{P}}$. The pressure tensor is often split into an equilibrium part $p\mathbf{1}$ and a viscous part $\boldsymbol{\Pi}$:

$$\mathbf{P} = p\mathbf{1} + \boldsymbol{\Pi}, \tag{A5}$$

p being the equilibrium pressure. The viscous part is then decomposed into a traceless symmetric part $\overset{os}{\boldsymbol{\Pi}}$ and an antisymmetric part $\overset{a}{\boldsymbol{\Pi}}$:

$$\boldsymbol{\Pi} = \Pi\mathbf{1} + \overset{os}{\boldsymbol{\Pi}} + \overset{a}{\boldsymbol{\Pi}}, \tag{A6}$$

where $\Pi = \mathrm{tr}(\boldsymbol{\Pi})/3$. It is important to note that $\overset{a}{\boldsymbol{\Pi}}$ is equal to $\overset{a}{\mathbf{P}}$, which means that the vector dual $\overset{d}{\boldsymbol{\Pi}}$ of $\overset{a}{\boldsymbol{\Pi}}$ is given by Eq. (A4). Likewise, the couple tensor is decomposed into traceless symmetric and antisymmetric parts:

$$\mathbf{Q} = Q\mathbf{1} + \overset{os}{\mathbf{Q}} + \overset{a}{\mathbf{Q}}. \tag{A7}$$

The vector dual of $\overset{a}{\mathbf{Q}}$ is denoted $\overset{d}{\mathbf{Q}}$. The linear constitutive equations that relate the forces and the conjugate fluxes in the balance equations are then written as [1,6]

$$\Pi = -\eta_v(\nabla \cdot \mathbf{u}), \tag{A8}$$

$$\overset{os}{\boldsymbol{\Pi}} = -2\eta_0(\overset{os}{\nabla\mathbf{u}}), \tag{A9}$$

$$\overset{d}{\boldsymbol{\Pi}} = -\eta_r(\nabla \times \mathbf{u} - 2\mathbf{w}), \tag{A10}$$

$$Q = -\zeta_v(\nabla \cdot \mathbf{w}), \tag{A11}$$

$$\overset{os}{\mathbf{Q}} = -2\zeta(\overset{os}{\nabla\boldsymbol{w}}), \tag{A12}$$

$$\overset{d}{\mathbf{Q}} = -\zeta_r(\nabla \times \mathbf{w}). \tag{A13}$$

Here η_v is the bulk viscosity, η_0 is the shear viscosity, η_r is the vortex (or rotational) viscosity, ζ_v, ζ, and ζ_r are the equivalent vortex spin viscosities, and $\mathbf{w}$ is the streaming angular velocity. Note that in the presence of temperature gradients cross-coupling terms appear in the constitutive relations [6]. The thermodynamic force $\nabla \times \mathbf{u} - 2\mathbf{w}$ is sometimes referred to as the sprain rate [33]. Substituting the constitutive relations into the balance equations, assuming constant transport coefficients and the absence of applied external torque, we obtain the corresponding Navier-Stokes equations [1,6]:

$$\rho\frac{d\mathbf{u}}{dt} = \rho\mathbf{F}_e - \nabla p + (\eta_v + \eta_0/3 - \eta_r)\nabla(\nabla \cdot \mathbf{u}) + (\eta_0 + \eta_r)\nabla^2\mathbf{u} + 2\eta_r(\nabla \times \mathbf{w}), \tag{A14}$$

$$\rho\frac{d\mathbf{s}}{dt} = 2\eta_r(\nabla \times \mathbf{u} - 2\mathbf{w}) + (\zeta_v + \zeta/3 - \zeta_r)\nabla(\nabla \cdot \mathbf{w}) + (\zeta + \zeta_r)\nabla^2\mathbf{w}. \tag{A15}$$

This, together with Eq. (A1) and an appropriate equation of state, completes the fluid dynamical description.

[1] S. R. de Groot and P. Mazur, *Non-Equilibrium Thermodynamics* (Dover Publications, New York, 1984).
[2] D. J. Evans and G. P. Morriss, *Statistical Mechanics of Nonequilibrium Liquids* (Academic Press, New York, 1990).
[3] J. D. Anderson, *Computational Fluid Dynamics: The Basics with Applications* (McGraw-Hill, New York, 1995).
[4] A. C. Eringen, *Contribution to Mechanics* (Pergamon, Oxford, 1969).
[5] N. K. Ailawadi, B. J. Berne, and D. Forster, Phys. Rev. A **3**, 1462 (1971).
[6] D. J. Evans and W. B. Streett, Mol. Phys. **36**, 161 (1978).
[7] K. P. Travis, B. D. Todd, and D. J. Evans, Physica A **240**, 315 (1997).
[8] K. P. Travis and D. J. Evans, Phys. Rev. E **55**, 1566 (1997).
[9] J. Delhommelle and D. J. Evans, Mol. Phys. **100**, 2857 (2002).
[10] Y. Radzyner and D. C. Rapaport, Phys. Rev. E **57**, 5687 (1998).
[11] Y.-K. Lee, J. Deval, P. Tabeling, and C.-M. Ho, Proceedings of the 14th IEEE International Conference on Micro Electro Mechanical Systems, Interlaken, Switzerland, 2001 (IEEE, New York, 2001), pp. 483–486.
[12] J. Hansen, J. Ottesen, and A. Lemarchand, Mol. Phys. **31**, 963 (2005).
[13] D. J. Evans and H. J. M. Hanley, Phys. Rev. A **25**, 1771 (1982).
[14] F. A. Engelund, *Hydrodynamik—Newtonske Vædskers Mekanik* (Danmarks Tekniske Højskole, Lyngby, 1968).
[15] J. S. Hansen, P. J. Daivis, and B. D. Todd, J. Chem. Phys. **126**, 144706 (2007).
[16] J. Delhommelle, Mol. Phys. **100**, 3479 (2002).
[17] K. P. Travis, B. D. Todd, and D. J. Evans, Phys. Rev. E **55**, 4288 (1997).
[18] J. Zhang, J. S. Hansen, B. D. Todd, and P. J. Daivis, J. Chem. Phys. **126**, 144907 (2007).
[19] B. D. Todd, D. J. Evans, and P. J. Daivis, Phys. Rev. E **52**, 1627 (1995).
[20] D. Frenkel and B. Smit, *Understanding Molecular Simulation* (Academic Press, New York, 1996).
[21] J. D. Weeks, D. Chandler, and H. C. Andersen, J. Chem. Phys. **54**, 5237 (1971).
[22] K. Kremer and G. S. Grest, J. Chem. Phys. **92**, 5057 (1990).
[23] S. Nosé, Mol. Phys. **52**, 255 (1984).
[24] W. G. Hoover, Phys. Rev. A **31**, 1695 (1985).
[25] J. P. Hansen and I. R. McDonald, *Theory of Simple Liquids* (Academic Press, New York, 1986).
[26] M. P. Allen, Mol. Phys. **52**, 705 (1984).
[27] B. D. Todd and P. J. Daivis, Mol. Simul. **33**, 189 (2007).
[28] S. T. Cui, P. T. Cummings, and H. D. Cochran, Mol. Phys. **88**, 1657 (1996).
[29] P. J. Daivis and D. J. Evans, J. Chem. Phys. **100**, 541 (1994).
[30] D. Brown and S. Neyertz, Mol. Phys. **84**, 577 (1995).
[31] M. L. Matin, P. J. Daivis, and B. D. Todd, J. Chem. Phys. **113**, 9122 (2000).
[32] D. D. Coleman and H. Markovitz, J. Appl. Phys. **35**, 1 (1964).
[33] R. Edberg, D. J. Evans, and G. P. Morriss, Mol. Phys. **62**, 1357 (1987).